Journal of Atomic, Molecular, Condensed Matter & Nano Physics
Vol. 8, No. 2, pp. 113–132, 2021
ISSN 2582-8215
Published by RGN Publications

http://www.rgnpublications.com

DOI: 10.26713/jamcnp.v8i2.1774

Research Article

Energy Levels, Radiative Data and Collisional Excitation of Chlorine like Tungsten W^{57+}

Nupur Verma*[1], Alok K. S. Jha[2] and Man Mohan[3]

[1] *Department of Physics, Deen Dayal Upadhyaya College* (*University of Delhi*), *Delhi 110078, India*
[2] *School of Physical Sciences, Jawaharlal Nehru University, Delhi 110067, India*
[3] *Department of Physics & Astrophysics, University of Delhi, Delhi 110007, India*
***Corresponding author:** verma_nupur123@rediffmail.com

Received: September 2, 2021 **Accepted:** October 12, 2021

Communicated by: Md. Rizwan

Abstract. Extended computation of energy levels and radiative data such as transition wavelengths, transition probabilities, and oscillator strengths for *electric dipole* (E1) transitions are performed for chlorine-like Tungsten ions WLVIII using the fully relativistic *Flexible Atomic Code* (FAC). Comparisons are done with the accessible experimental results and theoretical data in the literature. Close agreement has been found ensuring the accuracy and reliability of our results. We have studied collisional excitation cross section and presented magnetic sublevel cross sections for excitations from the ground state $3s^2\ 3p^5\ {}^2P^o{}_{3/2}$ to the first excited state $3s^2 3p^4 3d\ {}^4D_{3/2}$ of W^{57+} as a function of incident electron energy. We calculate new data for several levels where no other theoretical and/or experimental results are available. Our work will help to develop diagnostics for evaluating tungsten concentrations in fusion plasmas and provide platform for modeling predictions.

Keywords. Transition probabilities, Oscillator strengths, Excitation cross section

PACS. 32.70.Cs; 34.80.Dp

1. Introduction

Atomic data are needed for estimating the energy loss through impurity ions in fusion plasmas including modeling and diagnostics of plasmas. In current and future fusion devices there will be a variety of impurity ions present. Some elements are likely to invade the plasma through corrosion of plasma facing components, some will penetrate due to injection of material for

diagnostic purposes and some will infiltrate through inevitable contamination. These materials will have distinct spectral signatures and will, in some cases, be very effective radiators of energy, resulting in cooling of plasma. Hence, an explicit atomic database is required for distinguishing highly ionized impurity ions in fusion reactors and judging plasma temperature in existing magnetically confined fusion plasmas e.g. tokamaks, pinches and stellartors. The study of tungsten ions is of immense importance as the special properties of tungsten such as high melting point, low sputtering yield and low metal pressure allow it to be used as a potential plasma facing material in present-day large tokamaks, such as JET (*Joint European Torus*) and ITER (*International Thermonuclear Experimental Reactor*). Relativistic atomic data for highly charged tungsten ions such as energy levels and radiative decay rates are beneficial to access and control the radiation loss. Tungsten ions cause strong X-ray radiation over a broad range of temperatures as they are not completely ionized, even in the hot core as they move into a tokamak. Considering that electron induced processes are expected to play an important role, it is anticipated that tungsten ions will get excited by collision with plasma electrons and thereby decay by emitting radiation. Therefore, knowledge of electron impact cross section will aid in a detailed study of spectra for plasma diagnostics. Furthermore, the magnetic sublevel cross sections assist in the study of polarization of radiation emitted after decay of the excited states.

Chlorine like ions have been studied extensively in the past both experimentally and theoretically. Atomic structure codes have been used by Fawcett (Ar II-Fe X) [11], Hibbert [18], Aggarwal *et al*. [2], Goyal *et al*. [12], Verma *et al*. (Co XI) [28], Bhatia [5], and Berrington [4] to report atomic data for Cl-like ions. Experimentally, the spectra of different Cl-like ions have been studied using different light sources [10,17,26]. There is substantial previous experimental and theoretical work on atomic structure calculations of chlorine-like tungsten ions, which is a clear indicator of their significance in both theoretical and applied atomic physics, including fusion applications. Ralchenko *et al*. [24] studied extreme ultraviolet (EUV) spectra (4-20 nm) of Ca-like tungsten ions W^{54+} to Na-like tungsten ions W^{63+} obtained with an *electron beam ion trap* (EBIT). Using the *general-purpose relativistic atomic structure package* (GRASP) and the *flexible atomic code* (FAC), Aggarwal *et al*. [1] calculated excitation energies, radiative rates, and lifetimes for transitions in W^{57+} ions [1]. Priti *et al*. [21] reported the electron impact excitation due to $3s_{1/2}$-$3p_{3/2}$ and $3p_{1/2}$-$3d_{3/2}$ transitions in W^{n+} ($n = 44 - 66$) ions and magnetic sublevel excitation cross-sections were calculated for the above within the framework of fully relativistic distorted wave approach. Dipti *et al*. [9] considered M-shell electron impact excitation for specific magnetic sublevels in Fe-like W^{48+} through Al-like W^{61+} ions. Using the fully relativistic Dirac Fock method, Puri *et al*. [25] obtained the radiative data for forbidden ($M1$,$E2$) lines within the $3p^k$ ground configurations of highly charged tungsten ions from W^{57+} to W^{60+}. Xu *et al*. [29] reported excitation energies, wavelengths and transition probabilities for M shell excited states with partially filled 3p subshell in Cl-like tungsten using GRASP code. Koziol [15] investigated the radiative transitions for the $3p_{3/2}$-$3p_{1/2}$ fine splitting in Cl-like tungsten ions. More recently, Zhang *et al*. [30] systematically investigated the atomic properties of $n = 3$ states of the W^{56+}-W^{61+} ions using the second-order many-body perturbation theory, and the multi-configuration Dirac-Hartree-Fock method along with the relativistic configuration interaction approach. A comprehensive compilation of the results on spectral lines of chlorine-like tungsten W^{57+} ions can be seen in refs. [3,6–8,14,16,22,23,27].

The present work is an extension of our earlier work on W^{57+} ions. In our previous work, we carried out multi-configurational Dirac-Fock atomic structure calculations for chlorine-like tungsten ions and reported radiative data for $E1$, $E2$, $M1$, and $M2$ transitions [19]. In this paper, we have adopted the fully relativistic FAC (*Flexible Atomic Code*) utilizing the modified multiconfigurational *Dirac-Hartree-Fock-Slater* (DHFS) method to generate the wave functions. This code was originally developed by Gu [13] at Stanford University and used for its speed, multi-utility, and collisional radiative modeling. We present our computed energy levels, oscillator strengths, and transition probabilities for all electric-dipole-allowed ($E1$) transitions from the lowest five levels to the first 100 excited levels of W LVII using the FAC code. These results are compared with data compiled by NIST and our previous work on these ions, and other available theoretical data for the determination of accuracy. Our calculated energy levels agree closely with the NIST results, giving credibility to the correctness of our wave functions.

Most of the studies performed in the past on chlorine-like tungsten ions involve the data on excitation energies and radiative rates. However, not much examination has been done for electron-impact excitation of these ions, which is one of the most dominant research subjects today as collisional data is highly important for astrophysics, laser physics, fusion science, material science and most importantly, for modeling and characterization of a variety of plasmas. Therefore, reliable and detailed cross sectional data for fine structure transitions in a broad range of energy needs to be urgently studied to calculate correct plasma parameters. It is important to note here that there is no data on the explicit experimental measurements of electron impact excitation cross sections for fine structure transitions from the ground state to the first excited state in W LVIII therefore; theoretical predictions are of fundamental significance. Hence, the motivation for this work. In continuation of such effort, in our present work we mainly focus on the magnetic sublevel cross sections for excitation from the ground state i.e. $3s^2 3p^5\ {}^2P^o_{3/2}$to the first exited state $3s^2 3p^4({}^3P)3d\ {}^4D_{3/2}$ as a function of incident electron energy in the scheme of fully *relativistic distorted wave* (RDW) approximation theory.

2. Theoretical Method

We have obtained our results using the fully relativistic approach used in the well-established *Flexible Atomic Code* (FAC) of Gu [13]. We present a brief explanation of the theoretical approach applied in FAC. We get the energy levels of an N-electron atom by diagonalizing the relativistic Hamiltonian H,

$$H = \sum_{i=1}^{N} H_D(i) + \sum_{i<j}^{N} \frac{1}{r_{ij}}, \tag{2.1}$$

where $H_D(i)$ is the single-electron Dirac Hamiltonian. Here, the basis states ϕ_i which are generally cited as *configuration state functions* (CSF) are antisymmetric sums of products of N one-electron Dirac spinors $\varphi n\kappa m$

$$\varphi_{n\kappa m} = \frac{1}{r} \begin{Bmatrix} P_{n\kappa}(r)\chi_{\kappa m}(\theta,\phi,\sigma) \\ iQ_{n\kappa}(r)\chi_{-\kappa m}(\theta,\phi,\sigma) \end{Bmatrix}, \tag{2.2}$$

where $\chi_{\kappa m}$ is the standard spin-angular function; κ is the relativistic angular quantum number n is the principal quantum number; m is the z-component of the total angular momentum j.

Further, the approximate atomic state functions are computed by mixing the basis states using the identical symmetries

$$\Psi = \sum_v b_v \phi_v \tag{2.3}$$

b_v are the mixing coefficients ascertained after diagonalizing the total Hamiltonian.

Choice of Local Central Potential

The one-electron radial orbital have to be established in order to construct the Hamiltonian matrix. According to the conventional Dirac-Fock-Slater technique, the large and small components, P_{nk} and Q_{nk}, satisfy the coupled Dirac equation for a local central field $V(r)$

$$\left(\frac{d}{dr} + \frac{k}{r}\right) P_{nk} = \alpha \left(\varepsilon_{nk} - V + \frac{2}{\alpha^2}\right) Q_{nk},$$
$$\left(\frac{d}{dr} - \frac{k}{r}\right) Q_{nk} = \alpha (-\varepsilon_{nk} + V) P_{nk}, \tag{2.4}$$

where ε_{nk} are the energy eigenvalues of the radial orbital α is the fine structure constant.

The radial orbitals have an explicit effect on the potential, so the eq. (2.4) needs a self-consistent iteration. The orbitals from the preceding step are utilized to obtain the potential in each iteration. Accordingly, solving the eigenvalue problem using known potential is sufficing. Henceforth, eq. (2.4) is converted to a Schrodinger-like equation via two steps: elimination of the small component and carrying out the conversion

$$Pa = \xi_a(r) Fa(r),$$
$$\xi_a = \sqrt{1 + \alpha^2 [\varepsilon_a - V(r)]/2},$$
$$Q_a = \frac{\alpha}{2\xi_a^2} \left(\frac{d}{dr} P_a + \frac{\kappa}{r} P_A\right) \tag{2.5}$$

Within this conversion, we have

$$\frac{d^2}{dr^2} F_a(r) + \left\{2[\varepsilon_a - U(r)] - \frac{\kappa(\kappa+1)}{r^2}\right\} F_a(r) = 0 \tag{2.6}$$

where $U(r)$ is an effective potential defined as

$$U(r) = V(r) - \frac{\alpha^2}{2}\{[V(r) - \varepsilon_a]^2 - W(r)\}$$
$$W(r) = \frac{1}{4\xi^2(r)} \left[\frac{d^2}{dr^2} V(r) + \frac{3\alpha^2}{4\xi^2(r)} \left(\frac{d}{dr} V(r)\right)^2 - \frac{2\kappa}{r} \frac{d}{dr} V(r)\right]. \tag{2.7}$$

We apply the standard Numerov method to solve eq. (2.6). At the same time, it is essential to perform another transformation before pursuing the solution

$$t = t(r)$$
$$F_a(r) = \left(\frac{dt}{dr}\right)^{-\frac{1}{2}} G_a(t), \tag{2.8}$$

where $t(r)$ as a function of radial distance is judiciously selected so that a uniform grid can be applied in the new variable t, and the corresponding conversion on the wave function is to bring the differential equation for $G_a(t)$ to a Schrodinger-like formation, i.e., minus the first

derivative term

$$\frac{d^2}{dt^2}G_a(r) = \left(\frac{dt}{dr}\right)^{-2} G_a(t)\left\{\frac{\kappa(\kappa+1)}{r^2} - 2[\varepsilon_a - U(r)] + \frac{1}{2}\left(\frac{dt}{dr}\right)^{-1}\frac{d^3t}{dr^3} - \frac{3}{4}\left(\frac{dt}{dr}\right)^{-2}\left(\frac{d^2t}{dr^2}\right)^2\right\}. \quad (2.9)$$

It is noted that, for free orbitals with suitably high energy, solving eq. (2.9) in a customary way becomes unrealistic. We adopt a distinct technique for continuum states i.e. the phase amplitude approach.

The minimum and maximum radial distances, $r_{\min}$ and $r_{\max}$, modeling the radial grid are selected as

$$r_{\min} = \frac{10^{-6}}{Z_{eff}},$$
$$r_{\max} = \frac{500}{Z_{eff}}, \quad (2.10)$$

where Z_{eff} is the residual charge of the atomic ion that the electrons experience at large r.

Electron impact excitation is studied by implementing the distorted wave Born approximation in FAC as it is the most accurate method, wherein free orbitals are computed in a real potential bringing into consideration the electronic structure of the target ion, with minimal increase in complexity. Accurate description of target wave functions is an essential constituent of any dependable excitation cross section computation. The qualitative evaluation of the wave functions of the target ion is carried out by comparison of our computed excitation energies with the corresponding values obtained from measurements and other credible theoretical techniques.The total excitation cross sections are important whenever the electron distribution functions are isotropic. At the same time, magnetic sublevel excitation assumes significance where aligned excitation produces polarized line emission. One needs to calculate accurate magnetic sublevel cross-sections between sublevels of lower states and upper states to ascertain the degree of polarization, as well as the angular distribution of emitted lines, as a result of electron collisional excitation.

3. Results and Discussion

3.1 Energy Levels

The inclusion of different relativistic operators plays a significant role in the computation of energy levels and further calculation of other variables. Nevertheless, it may be noted that it is equally essential to include all the importance configuration interactions to form an appropriate correlation model for precise calculations. In our present computations, we have examined the effect of configuration interaction systematically by adding correlations missed in our earlier work [19]. In the previous work, we included configuration interaction among 15 configurations, namely [$1s^2 2s^2 2p^6$] $3s^2 3p^5$, $3s3p^6$, $3s^2 3p^4 3d$, $3s^2 3p^4 4*1$, $3s3p^5 3d$, $3s^2 3p^3 3d^2$, $3s3p^4 3d^2$, $3p^6 3d$, $3s^2 3p^2 3d^3$, $3p^5 3d^2$, $3s^2 3p^3 4d^2$, and $3s^2 3p^3 4f^2$, which generate 1163 levels. We exclude the core $1s^2 2s^2 2p^6$ [Ne] from the configuration notation. These correlations include single electron excitation from 3s orbital and 3p orbital for $3s^2 3p^5$ configuration, and also take into account double electron excitations from $n = 3$ orbital to possible incorporations of one or two electrons in the shells up to $n = 4$ orbital to form the basis set. Further work has been done by Aggarwal *et al*. [1] by including 44 configurations namely, $3s^2 3p^4 3d$, $3s3p^6$, $3s^2 3p^2 3d^3$, $3s3p^4 3d^2$, $3p^6 3d$,

$3s3p^23d^4$, $3s^23p^44*1$, $3s^23p^33d4*1$, $3s3p^54*1$, $3s^23p^45*1$, $3p^64*1$, $3s3p^55*1$, $3s^23d^5$, $3p^23d^5$, $3s3d^6$, $3d^7$, $3s^23p^5$, $3s^23p^33d^2$, $3s3p^53d$, $3s3p^33d^3$, $3s^23p3d^4$, $3p^53d^2$, $3s3p3d^5$ and $3p3d^6$, wherein excitations from $n = 3$ to $n = 5$ are also included. It is noted that recently Zhang *et al*. [30] included 10 configurations, $3s^23p^5$, $3s^23p^43d$, $3s^23p^33d^2$, $3s^23p^23d^3$, $3s3p^53d$, $3s3p^43d^2$, $3s3p^33d^3$, $3p^43d^3$, $3s3p^6$ and $3s3p^23d^4$ to study the excitation energies and wavelengths of W^{56+} to W^{61+} ions. In the present calculations, we include extensive configuration interaction among 56 configurations listed in Table 1. Here, we study the consequence of double electron excitation from 3s orbital to $n = 4$ orbital. The incorporation of these configurations significantly expands the size of the calculation, thereby generating 6929 levels. The inclusion of important configuration, such as $3p^43d^3$ (which was omitted in our previous calculations and work done by Aggarwal *et al*. [1]), generates new levels in the 140-207 Rydberg energy range. Increasing the amount of CI by adding configurations; $3s^23p^34*2$, $3p^53d4s$, $3p^54*2$ generates additional levels in a broad energy range up to 543 Rydberg.

Table 1. Configuration set used in the present FAC calculations

$3s^2\ 3p^5$	$3s^2\ 3p^3\ 3d\ 4p$	$3p^6\ 4p$
$3s^2\ 3p^4\ 3d^1$	$3s^2\ 3p^3\ 3d\ 4f$	$3p^6\ 4d$
$3s^2\ 3p^4\ 4s$	$3s^2\ 3p^2\ 3d^3$	$3p^6\ 4f$
$3s^2\ 3p^4\ 4p$	$3s^2\ 3p3d^4$	$3p^5\ 3d^2$
$3s^2\ 3p^4\ 4d$	$3s^23d^5$	$3p^5\ 3d\ 4s$
$3s^2\ 3p^4\ 4f$	$3s3p^6$	$3p^5\ 4s^2$
$3s^2\ 3p^3\ 3d^2$	$3s\ 3p^5\ 3d$	$3p^5\ 4p^2$
$3s^23p^3\ 4s^2$	$3s\ 3p^5\ 4s$	$3p^5\ 4d^2$
$3s^23p^3\ 4p^2$	$3s\ 3p^5\ 4p$	$3p^5\ 4f^2$
$3s^23p^3\ 4d^2$	$3s\ 3p^5\ 4d$	$3p^5\ 4s4p$
$3s^23p^3\ 4f^2$	$3s\ 3p^5\ 4f$	$3p^5\ 4s4d$
$3s^23p^3\ 4s4p$	$3s\ 3p^4\ 3d^2$	$3p^5\ 4s4f$
$3s^23p^3\ 4s4d$	$3s\ 3p^3\ 3d^3$	$3p^5\ 4p4d$
$3s^23p^3\ 4s4f$	$3s\ 3p^2\ 3d^4$	$3p^5\ 4p4f$
$3s^23p^3\ 4p4d$	$3s\ 3p\ 3d^5$	$3p^5\ 4d4f$
$3s^23p^3\ 4p4f$	$3s\ 3d^6$	$3p^4\ 3d^3$
$3s^23p^3\ 4d4f$	$3p^6\ 3d^1$	$3p^2\ 3d^5$
$3s^2\ 3p^3\ 3d^1\ 4s$	$3p^6\ 4s$	$3p^1\ 3d^6$
$3s^2\ 3p^3\ 3d^1\ 4d$	$3d^7$	

In Table 2, we compare our computed excitation energy levels (relative to the ground state) of the lowest 30 fine–structure levels of chlorine-like tungsten from FAC calculations, with the most recent NIST energy table [20]. The calculated values of our earlier work (2014) [19], Aggarwal and Keenan (2014) [1], Xu *et al*. (2017) [29], and Zhang *et al*. (2021) [30] are also presented for comparison. One can see that the agreement between our computed values and

the experimental values as complied in the NIST database is creditable. This can be attributed to the observation that most past calculations included limited CI with arbitrary choice of configurations. Our computed energy levels are consistent within 1% on comparison with the experimental values of NIST, the sole case where the disparity is more for the $3s3p^6\ ^2S_{1/2}$ level.

Table 2. Comparison of our computed excitation energies (in Rydberg) for the lowest 30 levels of W LVIII with the available theoretical and experimental values

Index	Configuration	Level	Energy (Ryd)					
			Present FAC	Mohan *et al.* [27]	Aggarwal *et al.* [11]	Xu *et al.* [13]	Zhang *et al.* [20]	NIST [14]
1	$3s^23p^5$	$^2P^o_{3/2}$	0.0000	0.0000	0.0000	0.0000	0.0000	0.0000
2	$3s^23p^4(^3P)\ 3d$	$^4D_{3/2}$	17.3480	17.3021	17.3139	17.2778	17.3347	17.3440
3	$3s^23p^4(^3P)\ 3d$	$^4D_{5/2}$	17.8035	17.7589	17.7689	17.7767	17.7860	17.7940
4	$3s^23p^4(^3P)\ 3d$	$^4P_{1/2}$	17.8642	17.8204	17.8298			17.8700
5	$3s^23p^4(^3P)\ 3d$	$^2F_{7/2}$	18.0719	18.0288	18.0365			18.0508
6	$3s^23p^4(^1S)\ 3d$	$^2D_{3/2}$	19.5077	19.4633	19.4739			19.4600
7	$3s^23p^4(^3P)\ 3d$	$^4D_{7/2}$	23.2707	23.2269	23.2348	23.0886		23.2796
8	$3s^23p^4(^3P)\ 3d$	$^4F_{9/2}$	23.4379	23.3937	23.4016	23.2301		23.4394
9	$3s^23p^4(^3P)\ 3d$	$^2P_{1/2}$	23.9254	23.8864	23.8917			24.0800
10	$3s^23p^5$	$^2P^o_{1/2}$	25.5554	25.5375	25.5590	25.6575		25.5040
11	$3s^23p^4(^1S)\ 3d$	$^2D_{5/2}$	25.5762	25.5710	25.5407			25.5000
12	$3s^23p^4(^3P)\ 3d$	$^4P_{3/2}$	26.0493	26.0159	26.0153		26.0095	26.1300
13	$3s^23p^4(^3P)\ 3d$	$^2D_{5/2}$	26.3614	26.3286	26.3320		26.3159	26.6000
14	$3s^23p^3(^2D)3d^2(^3F)$	$^2D^o_{3/2}$	35.7861		35.7203			
15	$3s^23p^3(^4S)3d^2(^1D)$	$^4D^o_{5/2}$	36.2351		36.1918			
16	$3s^23p^3(^2P)3d^2(^3F)$	$^4D^o_{1/2}$	36.2568		36.1709			
17	$3s^23p^3(^2D)3d^2(^3F)$	$^4H^o_{7/2}$	36.3801		36.3151			
18	$3s^23p^3(^2D)3d^2(^3P)$	$^4F^o_{3/2}$	38.0452		37.9659			
19	$3s3p^6$	$^2S_{1/2}$	39.8083	39.8073	39.8009	41.4911		41.2000
20	$3s^23p^3(^2D)3d^2(^3F)$	$^4H^o_{9/2}$	41.5264		41.4602			
21	$3s^23p^3(^2P)3d^2(^3F)$	$^4F^o_{7/2}$	41.8248		41.7572			
22	$3s^23p^4(^3P)\ 3d$	$^4D_{1/2}$	42.0580	42.0211	42.0280			42.2000
23	$3s^23p^3(^2P)3d^2(^3F)$	$^4D^o_{3/2}$	42.4778		42.4106			
24	$3s^23p^3(^2P)3d^2(^3P)$	$^2S^o_{1/2}$	42.5016		42.4321			
25	$3s^23p^3(^2P)3d^2(^3F)$	$^2F^o_{5/2}$	42.5858		42.5189			
26	$3s^23p^3(^2P)3d^2(^3P)$	$^4D^o_{5/2}$	42.6717		42.5991			
27	$3s^23p^3(^2D)3d^2(^1G)$	$^2I^o_{11/2}$	42.7977		42.7295			
28	$3s^23p^4(^3P)3d$	$^4F_{3/2}$	42.8444	42.8086	42.8123			42.9000
29	$3s^23p^3(^2P)3d^2(^3P)$	$^4D^o_{7/2}$	43.0611		42.9918			
30	$3s^23p^4(^3P)\ 3d$	$^4F_{5/2}$	43.4396	43.4053	43.4062			43.5000

Fine structure energy levels for the lowest 100 levels of W LVIII are reported in Table 3, which correspond to 56 configurations (as reported in Table 1) generating 6929 levels in

total (with energies upto 67 Ryd). The listed energy levels belong to $3s^23p^5$, $3s3p^6$, $3s^23p^43d$, $3s^23p^33d^2$, $3s^23p^23d^3$, and $3s3p^53d$ configurations. As can be seen in Table 3, we have presented results for many additional spectral lines, which have not been not reported in the latest NIST tables. New reported energy levels mostly correspond to the $3s^23p^33d^2$, $3s^23p^23d^3$, and $3s3p^53d$ configurations but energy for many new levels including $3s^23p^33d4*1$,$3s3p3d^5$, $3s^23p^44*1$, $3s^23d^5$, $3s^23p3d^4$, $3s^23p^34*2$, $3s3p^33d^3$, $3p^43d^3$, $3s3p^23d^4$ may be obtained electronically on request.

Table 3. Fine structure energies (in Rydberg) for the lowest 100 levels of Chlorine like Tungsten W LVIII using the FAC method

Index	Configuration	Level	Present energy
1	$3s^23p^5$	$^2P^o_{3/2}$	0.0000
2	$3s^23p^4(^3P)\ 3d$	$^4D_{3/2}$	17.3480
3	$3s^23p^4(^3P)\ 3d$	$^4D_{5/2}$	17.8035
4	$3s^23p^4(^3P)\ 3d$	$^4P_{1/2}$	17.8642
5	$3s^23p^4(^3P)\ 3d$	$^2F_{7/2}$	18.0719
6	$3s^23p^4(^1S)\ 3d$	$^2D_{3/2}$	19.5077
7	$3s^23p^4(^3P)\ 3d$	$^4D_{7/2}$	23.2707
8	$3s^23p^4(^3P)\ 3d$	$^4F_{9/2}$	23.4379
9	$3s^23p^4(^3P)\ 3d$	$^2P_{1/2}$	23.9254
10	$3s^23p^5$	$^2P^o_{1/2}$	25.5554
11	$3s^23p^4(^1S)\ 3d$	$^2D_{5/2}$	25.5762
12	$3s^23p^4(^3P)\ 3d$	$^4P_{3/2}$	26.0493
13	$3s^23p^4(^3P)\ 3d$	$^2D_{5/2}$	26.3614
14	$3s^23p^3(^2D\ )\ 3d\ ^2(^3F)$	$^2D^o_{3/2}$	35.7861
15	$3s^23p^3(^4S\ )\ 3d\ ^2(^1D)$	$^4D^o_{5/2}$	36.2351
16	$3s^23p^3(^2P\ )\ 3d\ ^2(^3F)$	$^4D^o_{1/2}$	36.2568
17	$3s^23p^3(^2D)\ 3d\ ^2(^3F)$	$^4H^o_{7/2}$	36.3801
18	$3s^23p^3(^2D)\ 3d\ ^2(^3P)$	$^4F^o_{3/2}$	38.0452
19	$3s3p^6$	$^2S_{1/2}$	39.8083
20	$3s^23p^3(^2D)\ 3d\ ^2(^3F)$	$^4H^o_{9/2}$	41.5264
21	$3s^23p^3(^2P)\ 3d\ ^2(^3F)$	$^4F^o_{7/2}$	41.8248
22	$3s^23p^4(^3P)\ 3d$	$^4D_{1/2}$	42.0580
23	$3s^23p^3(^2P)\ 3d\ ^2(^3F)$	$^4D^o_{3/2}$	42.4778
24	$3s^23p^3(^2P)\ 3d\ ^2(^3P)$	$^2S^o_{1/2}$	42.5016
25	$3s^23p^3(^2P)\ 3d\ ^2(^3F)$	$^2F^o_{5/2}$	42.5858
26	$3s^23p^3(^2P)\ 3d\ ^2(^3P)$	$^4D^o_{5/2}$	42.6717
27	$3s^23p^3(^2D)\ 3d\ ^2(^1G)$	$^2I^o_{11/2}$	42.7977
28	$3s^23p^4(^3P)\ 3d$	$^4F_{3/2}$	42.8444
29	$3s^23p^3(^2P)\ 3d\ ^2(^3P)$	$^4D^o_{7/2}$	43.0611
30	$3s^23p^4(^3P)\ 3d$	$^4F_{5/2}$	43.4396
31	$3s^23p^4(^1D)3d$	$^2G_{7/2}$	43.5414

(*Contd*. Table)

Index	Configuration	Level	Present energy
32	$3s^2 3p^3(^4S)3d^2(^1G)$	$^4G^o_{7/2}$	43.9448
33	$3s^2 3p^3(^4S)3d^2(^3P)$	$^4P^o_{5/2}$	44.0568
34	$3s^2 3p^3(^2P)3d^2(^1D)$	$^2P^o_{3/2}$	44.2709
35	$3s^2 3p^3(^4S)3d^2(^1G)$	$^4G^o_{9/2}$	44.5960
36	$3s^2 3p^3(^2P)3d^2(^3P)$	$^2D^o_{3/2}$	44.9118
37	$3s^2 3p^3(^2P)3d^2(^1G)$	$^2F^o_{5/2}$	45.4497
38	$3s^2 3p^3(^2P)3d^2(^3P)$	$^2P^o_{1/2}$	45.6022
39	$3s^2 3p^4(^1D)3d$	$^2F_{5/2}$	45.8778
40	$3s^2 3p^4(^1D)3d$	$^2P_{3/2}$	46.0619
41	$3s^2 3p^4(^1D)3d$	$^2S_{1/2}$	46,5775
42	$3s^2 3p^4(^3P)3d$	$^4F_{7/2}$	48.2926
43	$3s^2 3p^3(^2P)3d^2(^3F)$	$^4G^o_{11/2}$	48.4356
44	$3s^2 3p^3(^2P)3d^2(^1D)$	$^2D^o_{5/2}$	48.7484
45	$3s^2 3p^4(^1D)3d$	$^2D_{3/2}$	48.9820
46	$3s^2 3p^3(^2P)3d^2(^1D)$	$^2F^o_{7/2}$	49.1039
47	$3s^2 3p^3(^2P)3d^2(^3F)$	$^2F^o_{9/2}$	49.2652
48	$3s^2 3p^4(^1D)3d$	$^2G_{9/2}$	49.2657
49	$3s^2 3p^4(^3P)3d$	$^2F_{5/2}$	49.2851
50	$3s^2 3p^4(^1D)3d$	$^2D_{5/2}$	49.7944
51	$3s^2 3p^3(^2D)3d^2(^1D)$	$^2P^o_{1/2}$	50.1675
52	$3s^2 3p^4(^1D)3d$	$^2F_{7/2}$	50.4159
53	$3s^2 3p^3(^2D)3d^2(^3F)$	$^4F^o_{7/2}$	51.3439
54	$3s^2 3p^3(^2P)3d^2(^3F)$	$^2D^o_{5/2}$	51.6012
55	$3s^2 3p^3(^2P)3d^2(^1S)$	$^2P^o_{3/2}$	51.6720
56	$3s^2 3p^4(^3P)3d$	$^2D_{3/2}$	52.1562
57	$3s^2 3p^3(^2D)3d^2(^1S)$	$^2D^o_{3/2}$	52.5917
58	$3s^2 3p^4(^1D)3$	$^2P_{1/2}$	52.8667
59	$3s^2 3p^2(^3P)3d^3(^4F)$	$^6G_{3/2}$	55.3031
60	$3s3p^5(^3P)3d$	$^4P^o_{1/2}$	55.7304
61	$3s3p^5(^3P)3d$	$^4P^o_{3/2}$	56.8894
62	$3s3p^5(^3P)3d$	$^4F^o_{7/2}$	57.4532
63	$3s3p^5(^3P)3d$	$^4D^o_{5/2}$	57.6039
64	$3s3p^5(^1P)3d$	$^2P^o_{1/2}$	58.5742
65	$3s3p^5(^1P)3d$	$^2D^o_{3/2}$	59.0847
66	$3s3p^5(^1P)3d$	$^2F^o_{5/2}$	59.2676
67	$3s^2 3p^3(^4S)3d^2(^3F$	$^6F^o_{3/2}$	61.0730

(*Contd*. Table)

Index	Configuration	Level	Present energy
68	$3s^23p^3(^2D)3d^2(^3F$	$^4G^o_{5/2}$	61.0822
69	$3s^23p^2(^1S)3d^3(^4F)$	$^4F_{5/2}$	61.2385
70	$3s^23p^3(^2D)3d^2(^3F$	$^4G^o_{7/2}$	61.3672
71	$3s^23p^3(^4S)3d^2(^3F)$	$^6F^o_{1/2}$	61.5037
72	$3s^23p^2(^3P)3d^3(^4P)$	$^4P_{3/2}$	61.7449
73	$3s^23p^3(^2D)3d^2(^3F)$	$^2H^o_{9/2}$	61.8887
74	$3s^23p^2(^1S)3d^3(^2G)$	$^2G_{7/2}$	62.1825
75	$3s^23p^2(^3P)3d^3(^4P)$	$^6D_{1/2}$	62.1915
76	$3s3p^5(^3P)3d$	$^4F^o_{9/2}$	62.2018
77	$3s^23p^2(^1S)3d^3(^2H)$	$^2H_{9/2}$	62.2204
78	$3s^23p^3(^2P)3d^2(^3F)$	$^4G^o_{5/2}$	62.8287
79	$3s3p^5(^3P)3d$	$^2D^o_{5/2}$	63.3004
80	$3s3p^5(^3P)3d$	$^4D^o_{7/2}$	63.5944
81	$3s^23p^3(^4S)3d^2(^3P)$	$^6P^o_{3/2}$	63.8650
82	$3s3p^5(^3P)3d$	$^2D^o_{3/2}$	64.0148
83	$3s^23p^2(^1S)3d^3(^4P)$	$^4P_{5/2}$	64.1250
84	$3s3p^5(^1P)3d$	$^2F^o_{7/2}$	64.5276
85	$3s^23p^3(^2D)3d^2(^3F)$	$^4D^o_{5/2}$	64.5964
86	$3s^23p^3(^2D)3d^2(^3F)$	$^4P^o_{1/2}$	64.6670
87	$3s^23p^3(^4S)3d^2(^3F)$	$^2F^o_{7/2}$	64.8215
88	$3s^23p^3(^2D)3d^2(^3F)$	$^4D^o_{3/2}$	64.9114
89	$3s^23p^3(^2D)3d^2(^3P)$	$^4D^o_{5/2}$	65.3555
90	$3s3p^5(^1P)3d$	$^2D^o_{5/2}$	65.3895
91	$3s^23p^3(^4S)3d^2(^3F)$	$^6F^o_{9/2}$	65.9270
92	$3s^23p^3(^2D)3d^2(^3P)$	$^4P^o_{3/2}$	65.9659
93	$3s^23p^3(^4S)3d^2(^3F)$	$^6F^o_{5/2}$	66.0219
94	$3s^23p^3(^4S)3d^2(^3F)$	$^6F^o_{7/2}$	66.0308
95	$3s3p^5(^3P)3d$	$^2P^o_{1/2}$	66.2254
96	$3s^23p^3(^2P)3d^2(^3P)$	$^4D^o_{1/2}$	66.2933
97	$3s^23p^3(^2D)3d^2(^3P)$	$^4F^o_{7/2}$	66.5077
98	$3s^23p^3(^2P)3d^2(^1D)$	$^2D^o_{3/2}$	66.5117
99	$3s^23p^3(^4S)3d^2(^3P)$	$^6P^o_{5/2}$	66.5213
100	$3s^23p^3(^2D)3d^2(^3F)$	$^4H^o_{11/2}$	66.6156

3.2 Radiative Rates

Radiative transition rates are computed in a unique multipole approximation, where the initial state is given by $\psi_i = \sum v b_{iv} \Phi_v$. Final state is given by $\psi f = \sum \mu b_{f\mu} \Phi_\mu$ and the multipole operator is *OLM*. The second quantization technique is applied to resolve the Hamiltonian

matrix elements by recombination of the creation and annihilation operators by means of Racah algebra. Here, the weighted oscillator strength and transition rates are given by,

$$gf_{fi} = [L]^{-1}\omega(\alpha\omega)^{2L-2}S_{fi}, \tag{3.1}$$
$$gA_{fi} = 2\alpha^3\omega^2 gf_{fi},$$

S_{fi} being the generalized line strength of transition and $\omega = E_i - E_f$ is the transition energy.

In Table 4, we report wavelengths (λ in Å), weighted oscillator strengths (gf_{ij} dimensionless), and radiative rates (A_{ji} in s^{-1}) for all electric dipole ($E1$) transitions with $i \le 5$ and $j \le 100$ in W LVIII. We predict many new oscillator strengths and radiative rates which have not yet been experimentally discerned and will build ground for experimental work in future.

Table 4. Wavelengths (λ in Å), weighted oscillator strengths (gf_{ij} dimensionless), radiative rates (A_{ji} in s^{-1}) for W LVIII

i	j	λ	gf_{ij}	A_{ji}
1	2	235.8800	4.3299E-03	2.6134E+09
1	3	242.0784	9.7756E-03	4.1430E+09
1	4	242.9029	1.5465E-02	1.9796E+10
1	6	265.2641	2.3880E-03	1.8228E+09
1	9	325.3905	3.5763E-02	8.2153E+10
1	11	347.8531	3.7934E-04	3.3196E+08
1	12	354.2891	3.7195E-01	5.0646E+11
1	13	358.5349	7.5190E-01	6.9901E+11
1	19	541.4081	2.1216E-01	1.3493E+12
1	22	572.1159	9.0765E-03	6.4456E+10
1	28	582.8185	7.9598E-05	2.9331E+08
1	30	590.9165	4.3786E-02	1.1057E+11
1	39	624.0891	1.1291E+00	3.1804E+12
1	40	626.5947	7.5175E-01	3.2018E+12
1	41	633.5823	7.6444E-01	6.6578E+12
1	45	666.3476	2.0094E-03	9.6789E+09
1	49	670.4709	1.5582E-05	5.0657E+07
1	50	677.4002	8.5375E-04	2.8332E+09
1	56	709.5326	7.7450E-03	4.2298E+10
1	58	719.1933	3.1169E-03	3.4978E+10
1	59	752.0048	4.5255E-05	2.7763E+08
1	69	832.7823	1.3587E-07	6.8149E+05
1	72	839.6714	6.5731E-07	5.0273E+06
1	75	845.7479	5.5568E-09	8.6236E+04
1	83	872.0554	7.4139E-08	4.0775E+05

(*Contd.* Table)

i	j	λ	gf_{ij}	A_{ji}
2	14	250.7227	9.2490E-03	6.3071E+09
2	15	256.8317	1.4668E-03	6.9972E+08
2	16	257.1265	4.3374E-03	6.2216E+09
2	18	281.4601	3.8510E-04	3.3094E+08
2	23	341.7890	7.5505E-02	9.5685E+10
2	24	342.1126	2.7472E-02	6.9759E+10
2	25	343.2589	2.0169E-01	1.7186E+11
2	26	344.4285	1.0039E-02	8.6127E+09
2	33	363.2720	2.4608E-01	2.3486E+11
2	34	366.1866	1.5043E-01	2.1883E+11
2	36	374.9064	4.3182E-03	6.5842E+09
2	37	382.2251	2.0440E-02	2.1596E+10
2	38	384.3003	8.6547E-05	2.7731E+08
2	44	427.1262	4.1472E-04	5.4717E+08
2	51	446.4336	2.7567E-04	1.1920E+09
2	54	465.9421	9.8615E-05	1.5483E+08
2	60	521.9934	7.3989E-02	4.3740E+11
2	61	537.7612	1.6207E-01	5.0841E+11
2	63	547.4802	1.8223E-01	3.9501E+11
2	64	560.7441	4.5481E-02	3.1027E+11
2	65	567.6634	7.4517E-02	2.6049E+11
2	66	570.1332	1.9406E-01	4.5619E+11
2	67	594.7823	3.0552E-01	1.1725E+12
2	68	594.9299	3.5166E-01	9.0014E+11
2	71	600.6053	1.5097E-01	1.1816E+12
2	78	618.6912	1.1936E-01	3.3042E+11
2	79	625.0124	1.0421E-03	2.9442E+09
2	81	632.7953	2.5069E-01	1.0890E+12
2	82	634.7393	1.1159E-04	4.8772E+08
2	85	642.7449	2.4360E-01	7.2779E+11
2	86	643.6920	6.4270E-01	5.7776E+12
2	88	647.0221	1.2828E-02	5.8257E+10
2	89	653.0572	4.3246E-02	1.3339E+11
2	90	653.4689	7.0137E-04	2.1660E+09
2	92	661.3758	3.8173E-03	1.8113E+10
2	93	662.1620	1.8629E-02	5.9070E+10

(*Contd*. Table)

i	j	λ	gf_{ij}	A_{ji}
2	95	664.8182	1.8602E-02	1.7838E+11
2	96	665.8250	9.1230E-05	8.7748E+08
2	98	668.7895	1.0504E-04	5.0967E+08
2	99	668.9441	4.6651E-03	1.5097E+10
3	14	244.5243	7.5397E-03	4.8904E+09
3	15	250.6333	1.0002E-03	4.5439E+08
3	17	252.6063	2.0461E-02	7.0815E+09
3	18	275.2617	1.5800E-02	1.2987E+10
3	21	326.7069	1.2704E-04	7.3548E+07
3	23	335.5905	2.5568E-02	3.1237E+10
3	25	337.0605	2.1454E-02	1.7627E+10
3	26	338.2301	2.3944E-03	1.9810E+09
3	29	343.5270	3.3630E-03	2.1526E+09
3	32	355.5515	7.4399E-01	5.1014E+11
3	33	357.0736	2.6859E-01	2.4766E+11
3	34	359.9882	4.5485E-04	6.3943E+08
3	36	368.7079	5.1568E-02	7.6050E+10
3	37	376.0267	1.1904E-03	1.2172E+09
3	44	420.9278	1.6626E-04	2.1304E+08
3	46	425.7661	3.2952E-03	3.2399E+09
3	53	456.2426	1.4497E-03	1.6367E+09
3	55	460.7071	2.4595E-04	5.6630E+08
3	61	531.5628	1.3593E-01	4.1666E+11
3	62	539.2324	2.0577E-01	3.2453E+11
3	63	541.2817	4.3023E-01	9.1161E+11
3	65	561.4650	1.1900E-01	4.0695E+11
3	66	563.9348	4.0990E-02	9.4275E+10
3	67	588.5839	3.3735E-02	1.2678E+11
3	68	588.7315	1.4101E-01	3.5346E+11
3	70	592.6101	5.2609E-01	1.0021E+12
3	78	612.4928	4.2635E-02	1.1567E+11
3	79	618.8140	5.5690E-04	1.5422E+09
3	80	622.8126	1.3512E-03	2.8428E+09
3	81	626.5968	1.2343E-01	5.2571E+11
3	82	628.5409	1.1541E-02	4.9462E+10
3	84	635.5495	9.0496E-03	1.9827E+10

(*Contd*. Table)

i	j	λ	gf_{ij}	A_{ji}
3	85	636.5464	9.0687E-01	2.6574E+12
3	87	639.6011	2.9337E-01	6.5095E+11
3	88	640.8237	1.0684E+00	4.7594E+12
3	89	646.8587	5.1272E-02	1.5515E+11
3	90	647.2704	2.3832E-03	7.2210E+09
3	92	655.1774	6.0682E-04	2.8257E+09
3	93	655.9636	2.8434E-02	8.8481E+10
3	94	656.0681	5.9480E-03	1.3886E+10
3	97	662.5777	2.7752E-03	6.6082E+09
3	98	662.5911	6.1329E-02	2.9208E+11
3	99	662.7457	9.0698E-03	2.8810E+10
4	14	243.6998	7.0383E-03	4.5345E+09
4	16	250.1036	2.0103E-02	2.7283E+10
4	18	274.4372	1.6960E-03	1.3857E+09
4	23	334.7661	2.9645E-02	3.6040E+10
4	24	335.0897	3.1699E-02	7.7223E+10
4	34	359.1637	1.8464E-01	2.5838E+11
4	36	367.8835	1.2492E-01	1.8340E+11
4	38	377.2774	6.7849E-03	2.0953E+10
4	51	439.4107	2.1929E-03	9.1863E+09
4	60	514.9705	4.8151E-02	2.7705E+11
4	61	530.7383	4.6242E-02	1.4130E+11
4	64	553.7212	5.2040E-02	3.4618E+11
4	65	560.6405	2.5597E-02	8.7277E+10
4	67	587.7594	1.7715E-01	6.6386E+11
4	71	593.5824	3.4516E-01	2.6385E+12
4	81	625.7724	3.3084E-01	1.4054E+12
4	82	627.7164	1.2143E-04	5.1904E+08
4	86	636.6691	9.3381E-02	8.2123E+11
4	88	639.9992	2.3831E-01	1.0589E+12
4	92	654.3529	7.0403E-03	3.2701E+10
4	95	657.7953	8.4424E-03	7.9255E+10
4	96	658.8021	2.8159E-02	2.6516E+11
4	98	661.7666	2.2533E-02	1.0705E+11
5	15	246.9820	3.6529E-02	1.6115E+10
5	17	248.9550	4.8864E-03	1.6427E+09

(*Contd*. Table)

i	j	λ	gf_{ij}	A_{ji}
5	20	318.9956	5.2511E-04	2.3186E+08
5	21	323.0556	5.1752E-02	2.9295E+10
5	25	333.4092	3.5956E-02	2.8906E+10
5	26	334.5788	2.3745E-04	1.9224E+08
5	29	339.8757	2.1444E-01	1.3436E+11
5	32	351.9002	1.6819E-02	1.1297E+10
5	33	353.4223	2.2951E-02	2.0733E+10
5	35	360.7595	1.1686E+00	6.5996E+11
5	37	372.3754	6.1999E-02	6.2174E+10
5	44	417.2765	5.6685E-04	7.1380E+08
5	46	422.1148	2.9245E-04	2.8264E+08
5	47	424.3089	1.6670E-02	1.3023E+10
5	53	452.5913	1.3857E-04	1.5396E+08
5	54	456.0924	1.6994E-03	2.5566E+09
5	62	535.5811	5.0860E-01	7.9131E+11
5	63	537.6305	4.7808E-02	9.9936E+10
5	66	560.2835	4.2460E-01	9.6396E+11
5	68	585.0802	1.2219E-03	3.0251E+09
5	70	588.9588	6.0444E-02	1.1372E+11
5	73	596.0593	4.5252E-01	6.9763E+11
5	76	600.2097	1.6605E-03	2.5957E+09
5	78	608.8415	3.9249E-02	1.0522E+11
5	79	615.1627	2.5476E-03	6.9721E+09
5	80	619.1613	1.3431E-02	2.7928E+10
5	84	631.8982	8.3127E-02	1.8003E+11
5	85	632.8951	1.6773E-03	4.8588E+09
5	87	635.9498	2.1444E+00	4.7041E+12
5	89	643.2074	1.8110E+00	5.4184E+12
5	90	643.6191	1.9393E-02	5.8099E+10
5	91	651.0261	2.9776E-04	5.4761E+08
5	93	652.3123	6.7079E-02	2.0642E+11
5	94	652.4168	1.7758E-02	4.0999E+10
5	97	658.9264	1.8769E-02	4.4201E+10
5	99	659.0944	1.1027E-02	3.4642E+10

3.3 Electron Impact Excitation

In these calculations the underlying target structure is provided by FAC code [13]. The cross-section data validity depends on the precision of the target wave functions. These target wave functions are evaluated by comparing the computed excitation energies with the existing theoretical and experimental results. Based on the comparison with other theoretical work, our listed energy levels match much better with the NIST results considering the inclusion of all important CI in our calculations.

Electron impact cross section is calculated by integrating differential cross sectioned $d\sigma/d\Omega$ over the angles. Here, averaging is carried out over initial magnetic sublevels (M_i), such that we obtain the cross section for excitation to a specific magnetic sublevel (M_f). Due to time reversal symmetry, the cross section for $-M_i \rightarrow -M_f$ is the same as that for $M_i \rightarrow M_f$, only the cross sections with $M_i \leq 0$ are reported.

Figure 1 represents the total electron impact excitation cross section for excitation from the ground state i.e. $3s^2 3p^{52}P^o{}_{3/2}$to the first excited sate $3s^2 3p^4(^3P)3d\ ^4D_{3/2}$ as a function of incident electron energy in eV.

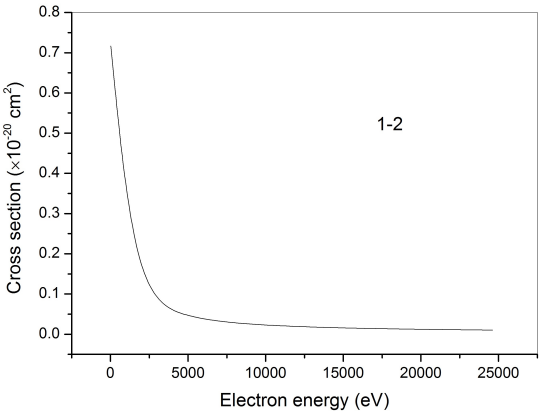

Figure 1. Total electron impact excitation cross section for excitation from the ground state i.e. $3s^2 3p^5\ ^2P^o{}_{3/2}$to the first excited sate $3s^2 3p^4(^3P)3d\ ^4D_{3/2}$

The ground state $3s^2 3p^5\ ^2P^o{}_{3/2}$splits into magnetic sublevels $M_i : \pm 3/2, \pm 1/2$. The excited state $^4D_{3/2}$ splits into magnetic sublevels $M_f : \pm 3/2, \pm 1/2$. Figure 2 denotes the magnetic sublevel cross section for excitation from $3s^2 3p^5\ ^2P^o{}_{3/2}$with initial magnetic sublevel $M_i = -3/2$ to $3s^2 3p^4(^3P)3d\ ^4D_{3/2}M_f$=±3/2, ±1/2 as a function of incident electron energy (in eV). It is noted that for the case where excitations take place from the same lower magnetic sublevel with $M_i = -3/2$, the cross sections for the magnetic sublevel with $M_f = -3/2$ are the highest which is followed by excitation to sublevels with $M_f = -1/2$, $M_f = 1/2$ and the least for $M_f = 3/2$.

Figure 3 corresponds to the magnetic sublevel cross section for excitation from $3s^2 3p^5\ ^2P^o{}_{3/2}$with initial magnetic sublevel $M_i = -1/2$ to $3s^2 3p^4(^3P)\ 3d\ ^4D_{3/2}M_f = \pm 3/2, \pm 1/2$ as a function of incident electron energy (in eV). We see here that for excitations from the same lower state $M_i = -1/2$, the cross section for the sublevel $M_f = 3/2$ is the least as compared to the others in this set. Magnetic sublevel with higher magnetic sublevel cross section is considered to be preferentially populated relative to the magnetic sublevel with lower magnetic sublevel cross section. It is noted here that each of the cross-section curve exhibits the predictable standard behavior for the dipole allowed transition to acquire the asymptotic shape for the considered range of energy. This noteworthy behavior of the deviation of magnetic sublevel cross-section plays a crucial part to develop suitable collisional radiative models needed for the diagnostics of high temperature plasma such as of the ITER tokomak. The electron impact excitation study helps to give insight into physical conditions of plasma and orientation of magnetic field inside plasma along with the calculation of linear polarization, level population and spectral line intensity.

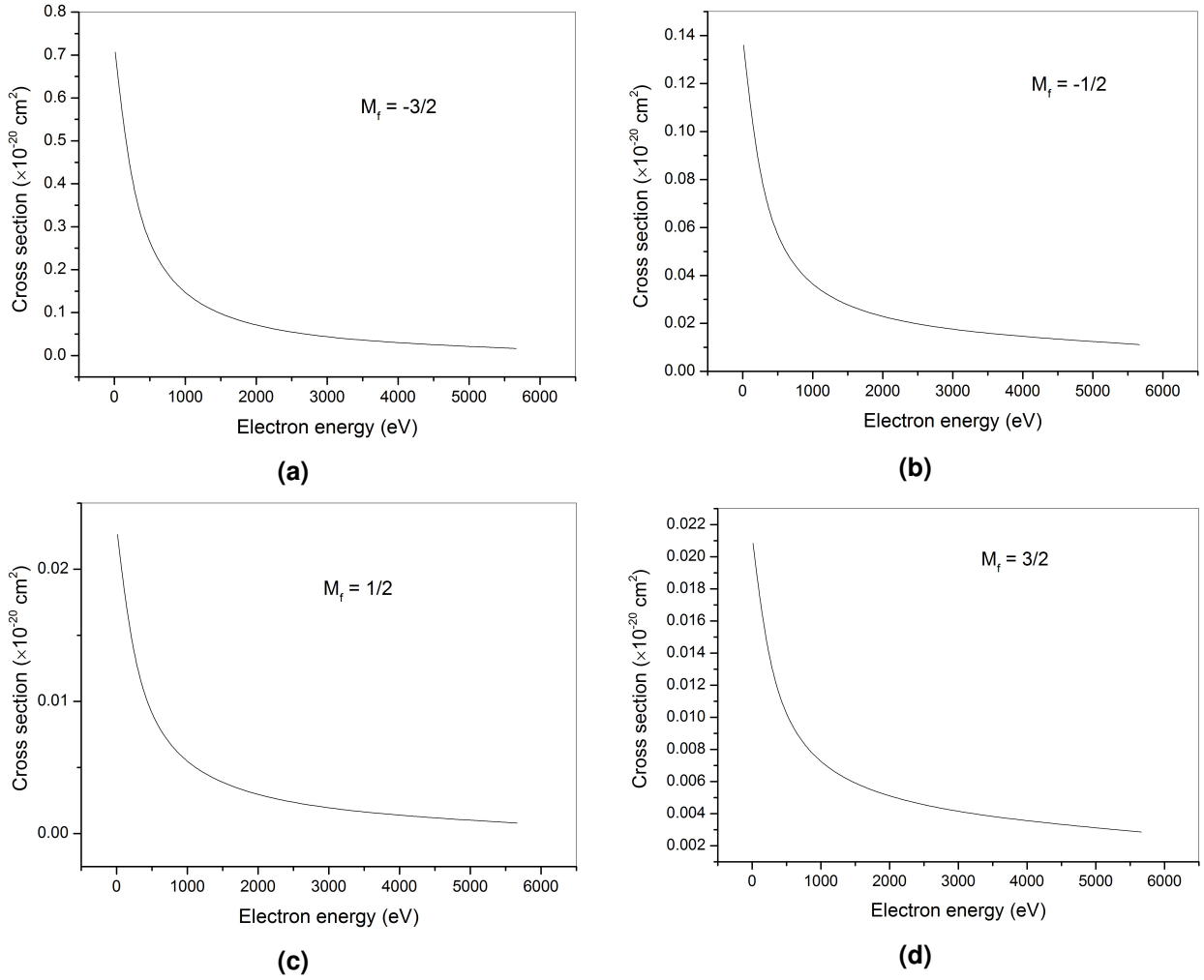

Figure 2. Magnetic sublevel cross section for excitation from the ground state $3s^2 3p^5\ ^2P^o{}_{3/2} M_i = -3/2$ to the excited state $3s^2 3p^4(^3P)3d\ ^4D_{3/2}$ (a) $M_f = -3/2$ (b) $M_f = -1/2$ (c) $M_f = 1/2$ (d) $M_f = 3/2$ as a function of incident electron energy (in eV)

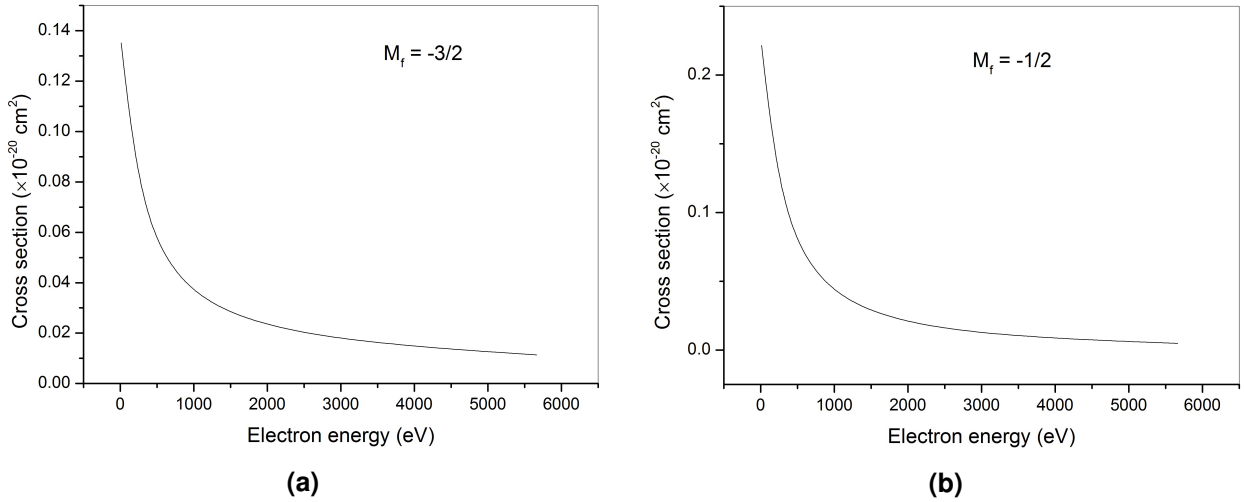

(*Contd*. Figure)

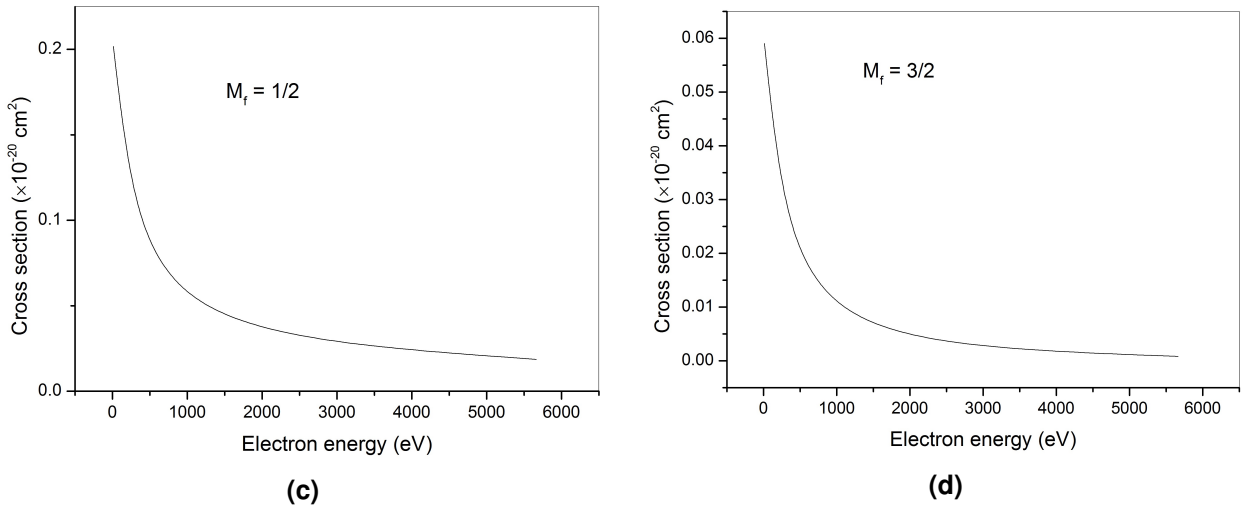

Figure 3. Magnetic sublevel cross section for excitation from the ground state $3s^2 3p^5\ ^2P^o{}_{3/2} M_i = -1/2$ to the excited state $3s^2 3p^4(^3P)3d\ ^4D_{3/2}$ (a) $M_f = -3/2$ (b) $M_f = -1/2$ (c) $M_f = 1/2$ (d) $M_f = 3/2$

4. Conclusion

In conclusion, we have utilized the fully relativistic Flexible atomic code with extensive CI to predict many additional spectral lines and atomic data for W LVIII. Good agreement between our computed fine structure energy levels and the theoretical and experimental results indicates the quality of computation of the wave functions. Exploring the Web pages, reliable databases reporting transition wavelengths and radiative rates in different ionic stages of W ions can be found. However, collisional data of highly charged tungsten ions is incomplete as calculations are complex and time consuming, given that W has high Z ($Z = 74$). In view of the scarce collisional data available, we have presented magnetic sublevel cross-section for excitation from the ground state to the first excited state of W^{57+} as a function of incident electron energy. Our study of electron impact excitation cross section will help investigations at the fusion reactor ITER, as well as devices ASDEX Upgrade and EBIT.

Competing Interests

The authors declare that they have no competing interests.

Authors' Contributions

All the authors contributed significantly in writing this article. The authors read and approved the final manuscript.

References

[1] K. M. Aggarwal and F. P. Keenan, Energy levels, radiative rates, and lifetimes for transitions in W LVIII, *Atomic Data and Nuclear Data Tables* **100**(6) (2014), 1603 – 1767, DOI: 10.1016/j.adt.2014.06.002.

[2] S. Aggarwal, J. Singh, A. K. S. Jha and M. Mohan, Photoionization cross-section of chorine-like iron, *Journal of Astrophysics and Astronomy* **33** (2012), 291 – 301, DOI: 10.1007/s12036-012-9151-7.

[3] P. Beiersdorfer, M. J. May, J. H. Scofield and S. B. Hansen, Atomic physics and ionization balance of high-Z ions: Critical ingredients for characterizing and understanding high-temperature plasmas, *High Energy Density Physics* **8** (2012), 271 – 283, DOI: 10.1016/j.hedp.2012.03.003.

[4] K. A. Berrington, J. C. Pelan and J. A. Waldock, Oscillator strength for $3s^2 3p^5$-$3s3p^6$ in Cl-like ions, *Journal of Physics B: Atomic, Molecular and Optical Physics* **34** (2001), L419, DOI: 10.1088/0953-4075/34/13/102.

[5] A. K. Bhatia and G. A. Doschek, Atomic data and spectral line intensities for Fe X, *Atomic Data and Nuclear Data Tables* **60** (1995), 97 – 143, DOI: 10.1006/adnd.1995.1005.

[6] M. Bilal, A. V. Volotka, R. Beerwerth and S. Fritzsche, Line strengths of QED-sensitive forbidden transitions in B, Al, F and Cl like ions, *Physical Review A* **97**(5) (2018), 052506, DOI: 10.1103/PhysRevA.97.052506.

[7] J. Clementson, P. Beiersdorfer, G. V. Brown, M. F. Gu, H. Lundberg, Y. Podpaly and E. Trabert, Tungsten spectroscopy at the Livermore electron beam ion trap facility, *Canadian Journal of Physics* **89** (2011), 571 – 580, DOI: 10.1139/p11-028.

[8] T. Das, L. Sharma and R. Srivastava, Electron impact excitation and polarization studies of Fe-like W^{48+} to Al-like W^{61+} ions, *Canadian Journal of Physics* **93** (2015), 888 – 897, DOI: 10.1139/cjp-2014-0636.

[9] Dipti, T. Das, L. Sharma and R. Srivastava, Electron impact excitation and polarization studies of Fe-like W^{48+} to Al-like W^{61+} ions, *Canadian Journal of Physics* **93**(8) (2015), 1 – 10, DOI: 10.1139/cjp-2014-0636.

[10] P. D. Dumont, H. P. Gornir, Y. Baudinet-Robinet and Kapenyak, Lifetime measurements in Ti IV-VII using transitions observed in beam-foil spectroscopy between 400 and 800 Å, *Journal of the Optical Society of America* **71** (1981), 502 – 503, DOI: 10.1364/JOSA.71.000502.

[11] B. C. Fawcett, Improved oscillator strength calculations for Ti VI and Fe X, *Atomic Data and Nuclear Data Tables* **47** (1991), 319 – 361, DOI: 10.1016/0092-640X(91)90004-N.

[12] A. Goyal, R. Sharma, A. K. Singh and M. Mohan, Fully relativistic atomic structure calculations for W XLIV for determination of plasma diagnostic terms, *Canadian Journal of Physics* **95** (2017), 950 – 957, DOI: 10.1139/cjp-2016-0812.

[13] M. F. Gu, The flexible atomic code, *Canadian Journal of Physics* **86**(5) (2008), 675 – 689, DOI: 10.1139/p07-197.

[14] K. N. Huang, Y. K. Kim and K. T. Cheng, Energy-level scheme and transition probabilities of Cl-like ions, *Atomic Data and Nuclear Data Tables* **28** (1983), 355 – 377, DOI: 10.1016/0092-640X(83)90022-0.

[15] K. Kozioł, Breit and QED contributions in atomic structure calculations of tungsten ions, *Journal of Quantitative Spectroscopy and Radiative Transfer* **242** (2020), 106772, DOI: 10.1016/j.jqsrt.2019.106772.

[16] A. Kramida, Recent progress in spectroscopy of tungsten, *Canadian Journal of Physics* **89** (2011), 551 – 570, DOI: 10.1139/p11-045.

[17] A. E. Livington, D. J. G. Irwin and E. H. Pinnington, Lifetime measurements in Ar II – Ar VII, *Journal of the Optical Society of America* **62** (1972), 1303 – 1308, DOI: 10.1364/JOSA.62.001303.

[18] M. Mohan and A. Hibbert, Level energies and oscillator strengths in Cu XIII, *Journal of Physics B: Atomic, Molecular and Optical Physics* **25** (1992), 4427, DOI: 10.1088/0953-4075/25/21/010.

[19] M. Mohan, S. Aggarwal and N. Singh, Multiconfigurational Dirac-Fock atomic structure calculations for Cl-like tungsten, *Canadian Journal of Physics* **92** (2014), 177 – 183, DOI: 10.1139/cjp-2013-0348.

[20] NIST Atomic Specra Database, website: `https://physics.nist.gov/PhysRefData/ASD/levels_form.html`.

[21] Priti, Dipti, L. Sharma and R. Srivastava, Fully relativistic electron impact excitation cross-section and polarization for tungsten ions, *Atoms* **3** (2015), 53 – 75, DOI: 10.3390/atoms3020053.

[22] T. Pütterich, R. Neu, R. Dux, A. D. Whiteford, M. G. O. Mullane and the ASDEX Upgrade Team, Modelling of measured tungsten spectra from ASDEX Upgrade and predictions for ITER, ASDEX Upgrade Team, *Plasma Physics and Controlled Fusion* **50** (2008), 085016, DOI: 10.1088/0741-3335/50/8/085016.

[23] P. Quinet, Dirac-Fock calculations of forbidden transitions within the $3p^k$ and $3d^k$ ground configurations of highly charged tungsten ions (W^{47+}-W^{61+}), *Journal of Physics B: Atomic, Molecular and Optical Physics* **44** (2011), 195007, DOI: 10.1088/0953-4075/44/19/195007.

[24] Y. Ralchenko, I. N. Draganic, J. N. Tan, J. D. Gillaspy, J. M. Pomeroy, J. Reader, U. Feldman and G. E. Holland, EUV spectra of highly-charged ions $W5^{4+}$-$W6^{3+}$ relevant to ITER diagnostics, *Journal of Physics B: Atomic, Molecular and Optical Physics* **41** (2008), 021003, DOI: 10.1088/0953-4075/41/2/021003.

[25] G. Singh and N. K. Puri, Revised and extended calculations of level energies, M1 and E2 radiative rates for highly charged Tungsten ions from W^{57+} to W^{60+}, *Journal of Physics B: Atomic, Molecular and Optical Physics* **49** (2016), 205002. DOI: 10.1088/0953-4075/49/20/205002.

[26] E. Träbert, Experimental checks on calculations for Cl-, S- and P-like ions of the iron group elements, *Journal of Physics B: Atomic, Molecular and Optical Physics* **29** (1996), L217 – 224, DOI: 10.1088/0953-4075/29/6/008.

[27] M. Vajed-Samii and K. MacDonald, Electric dipole transitions in Cl-like ions, *Atomic Data and Nuclear Data Tables* **26**(5) (1981), 467 – 475, DOI: 10.1016/0092-640X(81)90014-0.

[28] N. Verma, A. K. S. Jha and M. Mohan, Transitions in Co XI, *Journal of Physics B: Atomic, Molecular and Optical Physics* **38** (2005), 3185 – 3196, DOI: 10.1088/0953-4075/38/17/009.

[29] M. Xu, A. Y. Yan, S. A. Wu, F. Hu and X. F. Li, Wavelengths, transition probabilities, and oscillator strengths for M-shell transitions in tungsten ions with partially filled 3p subshell, *Canadian Journal of Physics* **95** (2017), 283 – 290, DOI: 10.1139/cjp-2016-0341.

[30] C. Y. Zhang, K. Wang, R. Si, M. Godefroid, P. Jönsson, J. Xiao, M. F. Gu and C. Y. Chen, Benchmarking calculations with spectroscopic accuracy of level energies and wavelengths in W LVII–W LXII tungsten ions, *Journal of Quantitative Spectroscopy and Radiative Transfer* **269** (2021), 107650, DOI: 10.1016/j.jqsrt.2021.107650.